

Phorbol 12-myristate 13-acetate-induced endocytosis of the Na-K-2Cl cotransporter in MDCK cells is associated with a clathrin-dependent pathway

Andreas Mykoniatis, Le Shen, Mary Fedor-Chaiken, Jun Tang, Xu Tang, Roger T. Worrell, Eric Delpire, Jerrold R. Turner, Karl S. Matlin, Patrice Bouyer and Jeffrey B. Matthews

Am J Physiol Cell Physiol 298:85-97, 2010. First published Oct 28, 2009;
doi:10.1152/ajpcell.00118.2009

You might find this additional information useful...

Supplemental material for this article can be found at:

<http://ajpcell.physiology.org/cgi/content/full/ajpcell.00118.2009/DC1>

This article cites 54 articles, 35 of which you can access free at:

<http://ajpcell.physiology.org/cgi/content/full/298/1/C85#BIBL>

Updated information and services including high-resolution figures, can be found at:

<http://ajpcell.physiology.org/cgi/content/full/298/1/C85>

Additional material and information about *AJP - Cell Physiology* can be found at:

<http://www.the-aps.org/publications/ajpcell>

This information is current as of December 25, 2009 .

Phorbol 12-myristate 13-acetate-induced endocytosis of the Na-K-2Cl cotransporter in MDCK cells is associated with a clathrin-dependent pathway

Andreas Mykoniatis,¹ Le Shen,² Mary Fedor-Chaiken,³ Jun Tang,¹ Xu Tang,¹ Roger T. Worrell,⁴ Eric Delpire,⁵ Jerrold R. Turner,² Karl S. Matlin,¹ Patrice Bouyer,¹ and Jeffrey B. Matthews¹

¹Departments of Surgery and ²Pathology, The University of Chicago, Chicago, Illinois; Departments of ³Cancer and Cell Biology and ⁴Molecular and Cellular Physiology, University of Cincinnati, Cincinnati, Ohio; and ⁵Department of Anesthesiology, Vanderbilt University Medical Center, Nashville, Tennessee

Submitted 16 March 2009; accepted in final form 27 October 2009

Mykoniatis A, Shen L, Fedor-Chaiken M, Tang J, Tang X, Worrell RT, Delpire E, Turner JR, Matlin KS, Bouyer P, Matthews JB. Phorbol 12-myristate 13-acetate-induced endocytosis of the Na-K-2Cl cotransporter in MDCK cells is associated with a clathrin-dependent pathway. *Am J Physiol Cell Physiol* 298: C85–C97, 2010. First published October 28, 2009; doi:10.1152/ajpcell.00118.2009.—In secretory epithelial cells, the basolateral Na⁺-K⁺-2Cl⁻ cotransporter (NKCC1) plays a major role in salt and fluid secretion. Our laboratory has identified NKCC1 surface expression as an important regulatory mechanism for Cl⁻ secretion in the colonic crypt cell line T84, a process also present in native human colonic crypts. We previously showed that activation of protein kinase C (PKC) by carbachol and phorbol 12-myristate 13-acetate (PMA) decreases NKCC1 surface expression in T84 cells. However, the specific endocytic entry pathway has not been defined. We used a Madin-Darby canine kidney (MDCK) cell line stably transfected with enhanced green fluorescent protein (EGFP)-NKCC1 to map NKCC1 entry during PMA exposure. At given times, we fixed and stained the cells with specific markers (e.g., dynamin II, clathrin heavy chain, and caveolin-1). We also used chlorpromazine, methyl- β -cyclodextrin, amiloride, and dynasore, blockers of the clathrin, caveolin, and macropinocytosis pathways and the vesicle “pinchase” dynamin, respectively. We found that PMA caused dose- and time-dependent NKCC1 endocytosis. After 2.5 min of PMA exposure, ~80% of EGFP-NKCC1 endocytic vesicles colocalized with clathrin and ~40% colocalized with dynamin II and with the transferrin receptor, the uptake of which is also mediated by clathrin-coated vesicles. We did not observe significant colocalization of EGFP-NKCC1 endocytic vesicles with caveolin-1, a marker of the caveolae-mediated endocytic pathway. We quantified the effect of each inhibitor on PMA-induced EGFP-NKCC1 endocytosis and found that only chlorpromazine and dynasore caused significant inhibition compared with the untreated control (61% and 25%, respectively, at 2.5 min). Together, these results strongly support the conclusion that PMA-stimulated NKCC1 endocytosis is associated with a clathrin pathway.

chlorpromazine; dynamin II; transferrin receptor

THE SODIUM-POTASSIUM-CHLORIDE COTRANSPORTER NKCC1 is an integral membrane cation-Cl⁻ cotransporter of the SLC12 family (SLC12A2) that is sensitive to the diuretic bumetanide (9a). NKCC1 is found in nearly all cell types and serves to regulate intracellular ionic composition and cell volume (44).

Address for reprint requests and other correspondence: J. B. Matthews, The Univ. of Chicago, 5841 S. Maryland Ave., MC 5029, Chicago, IL 60637 (e-mail: jmatthews@uchicago.edu) and P. Bouyer, The Univ. of Chicago, 5841 S. Maryland Ave., MC 5032, Chicago, IL 60637 (e-mail: pbouyer@uchicago.edu).

In secretory epithelial cells such as those lining the gastrointestinal and respiratory tracts, NKCC1 is located in the basolateral membrane, where it serves to accumulate intracellular Cl⁻ above its chemical equilibrium. This high intracellular Cl⁻ concentration is used to drive electrogenic salt secretion in a process gated by apical membrane Cl⁻ channels such as the CFTR (44). A dramatic reduction of the intestinal Cl⁻ secretion is observed in NKCC1^{-/-} mice (12) and in model secretory epithelia in which NKCC1 gene transcription is repressed (36).

NKCC1 appears to be an important independent regulatory site that may control overall epithelial secretory capacity. NKCC1 is a secondary active transporter, and, as such, its vectorial transport activity is, in large part, determined by transmembrane gradients of cotransported ions. However, NKCC1 transport activity is markedly enhanced by SPAK (Steo20p-related proline-alanine-rich kinase)- and WNK (with-no-lysine kinase)-dependent regulatory phosphorylation (9b, 14, 39a). A less well-characterized mechanism of control of NKCC1 activity involves its regulated endocytic retrieval from the basolateral membrane (37). Regulation of transport activity via endocytosis has been reported for a number of ion transporters, including the glutamate transporter (18), the Na⁺-Cl⁻ cotransporter (25), the Na⁺-HCO₃⁻ cotransporter (42), and ion channels (3, 32). Mechanistic details in many of these instances are lacking.

Multiple internalization pathways are known to exist (5, 40). Perhaps the best studied is the clathrin-mediated pathway. Molecular cargo that has a high affinity for its receptor is engulfed by a coated pit formed by a clathrin lattice. The coated pits invaginate and pinch off the membrane to form endocytic vesicles. A second pathway utilizes caveolin as a carrier for internalization (2, 5, 40). Caveolae are localized in cholesterol- and sphingolipid-rich domains of the plasma membrane. Members of the caveolin family of proteins form hairpin loops inserted into the inner leaflet of the membrane, where they promote the formation of endocytic vesicles. A nonclathrin or caveolin endocytosis mechanism also exists, but it remains poorly understood (5, 40). Macropinocytosis is a third pathway that accounts for internalization of large molecules from the extracellular space (5, 40). Macropinocytosis involves a series of intracellular signaling events mediated by Rho-family GTPases that regulate the assembly of actin to form a cell surface loop that fuses back with the plasma membrane to form the endocytic vesicle. Phagocytosis is another entry pathway utilized by macrophages or neutrophils to engulf large molecules (5, 40).

In our laboratory, we previously demonstrated that, in the Cl⁻ secretory human colonic cancer cell line T84, activation of

protein kinase C (PKC) by phorbol ester or the acetylcholine analog carbachol induces rapid endocytosis of NKCC1 and leads to a dramatic reduction in transepithelial Cl^- secretion (8, 11, 46). These findings were subsequently confirmed in native human colonic crypts (43). In the present study, we used a Madin-Darby canine kidney (MDCK) cell line stably transfected with an enhanced green fluorescent protein (EGFP)-tagged NKCC1 construct to map the internalization pathway of NKCC1 during PKC activation by PMA. We chose MDCK cells, because these cells are a well-defined model for the study of protein trafficking and are more amenable to genetic manipulation than intestinal cell lines. We found that PKC-dependent NKCC1 endocytosis is predominantly initiated by uptake via a dynamin- and clathrin-dependent mechanism.

MATERIALS AND METHODS

Reagents

Gel electrophoresis and immunoblotting reagents were obtained from Bio-Rad (Hercules, CA), enhanced chemiluminescence detection reagents from GE Healthcare (Piscataway, NJ), and protease inhibitor cocktail I from Calbiochem (San Diego, CA).

Primary rabbit anti-caveolin-1 antibodies were obtained from Abcam (Cambridge, MA), rabbit anti-clathrin heavy chain antibodies from Santa Cruz Biotechnology (Santa Cruz, CA), mouse anti-ZO-1 monoclonal antibody from Invitrogen (Carlsbad, CA), mouse anti- Na^+ - K^+ -ATPase α_1 -subunit from Millipore (Temecula, CA), rabbit polyclonal anti-CD71 anti-transferrin receptor (TfR) antibody from Novus Biologicals (Littleton, CO), and rabbit anti-dynamin II from Calbiochem. Mouse anti-NKCC1 monoclonal antibody T4, which was developed by Lytle et al. (29), was obtained from the Developmental Studies Hybridoma Bank operated under the auspices of the National Institute of Child Health and Human Development and maintained by the Department of Biological Sciences at the University of Iowa (Iowa City, IA). Rabbit anti-E-cadherin was generously provided by W. James Nelson (Stanford University, Palo Alto, CA). Alexa Fluor 594-conjugated phalloidin was used to stain F-actin, and Alexa Fluor 488 goat anti-mouse [anti-green fluorescent protein (GFP)] was used to amplify the signal from EGFP-NKCC1; both antibodies were obtained from Invitrogen. Goat anti-rabbit Alexa Fluor 594-conjugated secondary antibodies and SlowFade mounting medium were obtained from Invitrogen.

Chlorpromazine, amiloride, methyl- β -cyclodextrin, and dynasore were obtained from Sigma-Aldrich (St. Louis, MO). All other chemicals were of the highest grade available.

Cell Culture

The particular strain of MDCK cells used here is derived from cells originally cloned by Louvard (27) and referred to as the Heidelberg, or HD, strain. Cells (from passages 4–20) were cultured in high-glucose DMEM (GIBCO, Carlsbad, CA) supplemented with 5% FBS at 37°C in a 5% CO_2 atmosphere, as previously described (33), split every week (at 1:10 dilution) or twice a week (at 1:5 dilution), and fed every 3 days. For experiments, cells were cultured on rat tail collagen-coated Transwell inserts with 0.4- μm -diameter pores (Corning, NY) and allowed to grow to confluence for 4–6 days.

Establishment of Stable EGFP-NKCC1 MDCK Cell Line

Mapping the internalization pathway in T84 cells is complicated by their heterogenous morphology and the difficulty in stably expressing exogenous proteins. In contrast, because membrane trafficking pathways and machinery are well defined in MDCK cells, they are a very useful model for examining NKCC1 endocytosis (17, 26, 31). The MDCK cell strain used in our study (referred to as MDCK II) has a

low transepithelial resistance compared with the T84 cell line, but we found that this difference did not prima facie preclude examination of NKCC1 endocytosis. Indeed, preliminary experiments demonstrated that EGFP-NKCC1 is endocytosed in response to PMA when transiently expressed (data not shown). On the basis of these results, we engineered a stable EGFP-NKCC1 MDCK cell line for use in subsequent experiments.

MDCK cells were grown in high-glucose DMEM supplemented with 5% FBS and 10 mM HEPES-NaOH, pH 7.35, at 37°C in a 5% CO_2 atmosphere. Cells grown on six-well plates to ~60% confluence were transiently transfected with the mouse NKCC1 NH₂-terminal EGFP-tagged construct (14) with use of Lipofectamine 2000 (Invitrogen). Transfected cells were plated at $\sim 2 \times 10^6$ cells/cm² on 100-mm round plates, and positive colonies were selected using 0.17 mg/ml G418 and isolated by ring cloning. Six independent clones were propagated in the presence of 0.17 mg/ml G418, and three were selected as stable transfectants (A1, A2, and A3). In initial tests, all three independent cell lines yielded similar EGFP-NKCC1 internalization with PMA treatment. The A2 clone was further subcloned by dilution cloning, and a resulting subclone, A2-6, was used for most experiments. For convenience, these cells are referred to as EGFP-NKCC1 MDCK. The mean transepithelial resistance of the monolayers with EGFP-NKCC1 MDCK cells was $76.5 \pm 0.8 \Omega \cdot \text{cm}^2$ ($n = 20$) after 4 days in culture on Transwell inserts.

PMA Dose Determination

Previous work established that 100 nM PMA was the optimal working concentration for induction of endocytosis in T84 cells (35). We confirmed this in EGFP-NKCC1-expressing MDCK cells by quantifying NKCC1 endocytosis. To accomplish this, we counted endocytic vesicles visible 10 min after PMA addition in multiple high-power confocal fluorescence images generated from formaldehyde-fixed cells with use of Image J software. Using Image J software (W. S. Rasband, National Institutes of Health, Bethesda, MD; <http://rsb.info.nih.gov/ij/>, 1997–2009) and a custom macro using blur radii of 2 and 12 pixels, we processed micrographs with a difference-of-Gaussians spot-enhancing filter. This routine extracted spots and leveled background. Resulting features were counted using the Analyze Particles routine. We subjected cells to increasing doses of 1, 3, 10, 100, and 300 nM (prepared from a fresh 1 mM stock dissolved in DMSO) in complete culture medium to establish the dose-response curve (Fig. 1). As with T84 cells, 100 nM PMA was found to produce a

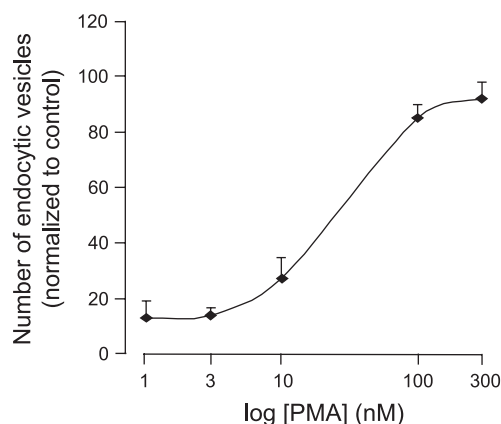


Fig. 1. PMA dose-response curve. Cultured Madin-Darby canine kidney (MDCK) cells expressing enhanced green fluorescent protein (EGFP)- Na^+ - K^+ - 2Cl^- cotransporter (NKCC1) on Transwell inserts were exposed to increasing PMA concentration for 10 min. Cells were fixed in paraformaldehyde and mounted for microscopy. Number of vesicles in the field of view was counted using Image J and normalized to control (vehicle-treated cells). Each point represents average of 4 different experiments.

maximum effect (plateau) and was chosen for our experiments. At higher concentrations, PMA dramatically alters the morphology of the cells.

Biotinylation Protocol

EGFP-NKCC1 MDCK cell monolayers grown to confluence on Transwell inserts (24 mm diameter) were treated with 100 nM PMA for 15 or 30 min at 37°C in culture medium. The cells were washed three times with ice-cold PBS supplemented with 0.1 mM CaCl₂ and 1.0 mM MgCl₂ (PBS⁺). Cells were then incubated basolaterally with 1 mg/ml *N*-hydroxysulfosuccinimidobiotin (sulfo-NHS biotin) for 15 min on ice. A fresh aliquot of sulfo-NHS biotin was added, and cells were incubated for an additional 15 min. Cells were washed five times with ice-cold PBS⁺ supplemented with 100 mM glycine as a quenching agent (16). The filters were excised and incubated in 1 ml of extraction buffer (1% Triton X-100, 150 mM NaCl, 5 mM EDTA, and 50 mM Tris, pH 7.40) supplemented with protease inhibitor cocktail I and 1 mM PMSF for 30 min on ice. Cells were scraped from the filter and centrifuged at 14,000 *g* at 4°C for 10 min. The supernatant was collected, and the protein concentration was determined using a bicinchoninic acid kit according to the manufacturer's instructions (Pierce Thermo Fisher Scientific, Rockford, IL). Samples containing an equal amount of protein were incubated with 100 μl of streptavidin-agarose beads (Pierce) overnight at 4°C on a shaker. The samples were spun for 1 min at 14,000 *g*, and the supernatants were discarded. The beads were washed three times with ice-cold extraction buffer: twice with a high-salt wash buffer (0.1% Triton X-100, 500 mM NaCl, and 50 mM Tris, pH 7.50) and once with a low-salt wash buffer (10 mM Tris, pH 7.50). The beads were resuspended in 40 μl of loading sample buffer (20 mM Tris, pH 6.80, β-mercaptoethanol, 0.01% bromophenol blue, and 1.0% SDS), boiled for 5 min, and analyzed by SDS-PAGE and Western blot.

Immunostaining

For immunostaining of EGFP-NKCC1 MDCK cell cultures, 6.5-mm-diameter Transwell inserts were used. Cells were treated with PMA or vehicle (DMSO). In some experiments, cells were preincubated with blockers of the different endocytosis pathways for times specified. Except as noted, cells were incubated in complete culture medium in a 5% CO₂ atmosphere. At the end of each experiment, monolayers were washed with cold PBS. Two different fixation methods were used. 1) Cells were fixed for 30 min in 3.7% paraformaldehyde dissolved in PBS, washed three times with PBS, and washed again with deionized water. Then the inserts were mounted on a coverslip with SlowFade mounting medium. 2) Cells were fixed in cold methanol for 10 min or overnight at -20°C. Then the cells were air-dried and rehydrated in PBS containing 0.1% *n*-octyl-glucopyranoside (PBS-og) and 100 μM bis(sulfosuccinimidyl) suberate for 30 min (45). Cells were washed three times in PBS-og, quenched for 15 min in 100 mM ethylenediamine at pH 7.50, and then rinsed in PBS-og. Cells were blocked in 1% nonfat dry milk, 1% fish gelatin, and 1% normal donkey serum in PBS-og for 1 h. Cells were incubated with primary antibody for 2 h at room temperature, washed five times in blocking buffer, and incubated with the secondary antibody for 1 h in blocking buffer. After five wash cycles, cells were rinsed with deionized water and mounted in SlowFade mounting medium.

In most of our experiments, we used the second fixation method, because we found that intracellular vesicular structures were better preserved for quantification (45).

For each primary antibody used for immunocytochemistry, we verified its specificity and cross-reactivity with canine proteins by Western blot analysis of MDCK cell extracts.

Microscopy

Live imaging (fluorescence multidimensional microscopy) was performed using an epifluorescence microscope (model DMLB, Leica

Microsystems, Bannockburn, IL) equipped with a ×100 HCX PL APO L U-V-I aqueous immersion objective [numerical aperture (NA) 0.9] and a 51022 filter set optimized for GFP (Chroma Technology, Rockingham, VT). The *z* stacks were collected in 0.25-μm steps with use of a motorized stage microscope and excitation filter wheels, *z* motor, and shutter (Ludl, Hawthorne, NY). Images were collected with a Retiga EXi camera (Q Imaging, Burnaby, BC, Canada) controlled by MetaMorph 7 software (Universal Imaging, Downingtown, PA).

Fixed and stained monolayers were imaged using the same microscope equipped with an 88000 filter set (Chroma Technology) and a ×100 (NA 1.35) PL APO oil immersion objective. The *z* stacks were collected at 0.25-μm intervals. Image stacks were deconvoluted using AutoDeblur X1 (Media-Cybernetics, Bethesda, MD). Confocal images were collected with a Zeiss LSM 510 confocal scanning microscope with a ×63 (NA 1.35) PL APO objective.

Morphometric Analysis

Deconvoluted *z* stacks were merged after pseudocolor assignment using MetaMorph. Vesicles were defined as round or oval structures present in at least two successive optical planes (0.25 μm apart). Because of the signal-to-noise ratio of the technique, vesicles less than five pixels in size were not counted. The number of vesicles in a single cell was counted over the full volume of the cell. We considered colocalization if there was >80% overlap between the signal of the two channels. For each measurement, 20 cells of an average shape and size were counted.

Statistical Analysis

Values are means ± SE, with *n* representing the number of experiments, followed by the number of cells examined at each time point. Each experiment was performed at least in duplicate, and data are representative of two or more independent studies. When relevant, data were analyzed by two-tailed Student's *t*-test, with *P* < 0.05 considered statistically significant.

RESULTS

Characterization of EGFP-NKCC1 Expression in MDCK Cells

To gain insight into the endocytosis of NKCC1 during PMA exposure, we used MDCK cells as a model of a polarized epithelium because of their well-characterized membrane traffic pathways (17, 27). To facilitate the mapping of internalization pathways in living and fixed cells, we employed MDCK cells stably expressing the NKCC1 NH₂-terminal EGFP-tagged construct (see MATERIALS AND METHODS). Previous work demonstrated that the EGFP-NKCC1 construct used here is capable of ion transport when expressed on the plasma membrane of *Xenopus* oocytes, suggesting that addition of EGFP to NKCC1 did not significantly affect its function (14).

In T84 cells and intestinal epithelial cells *in vivo*, NKCC1 is expressed on the basolateral plasma membrane. To confirm that this is also the case in MDCK cells expressing EGFP-NKCC1, we cultured cells to confluence on collagen-coated permeable supports for 3–4 days, fixed them in paraformaldehyde, and mounted them for confocal microscopy. As shown in Fig. 2, *A* and *B*, the middle plane *xy* optical section shows that the fluorescence signal of EGFP-NKCC1 is distributed along the lateral membrane of MDCK cells. Figure 2*B* further shows NKCC1 distribution in the plasma membrane, with phalloidin used to stain F-actin (red). An exclusive basolateral localization of EGFP-NKCC1 in polarized MDCK cell monolayers is demonstrated in *xz* images. We

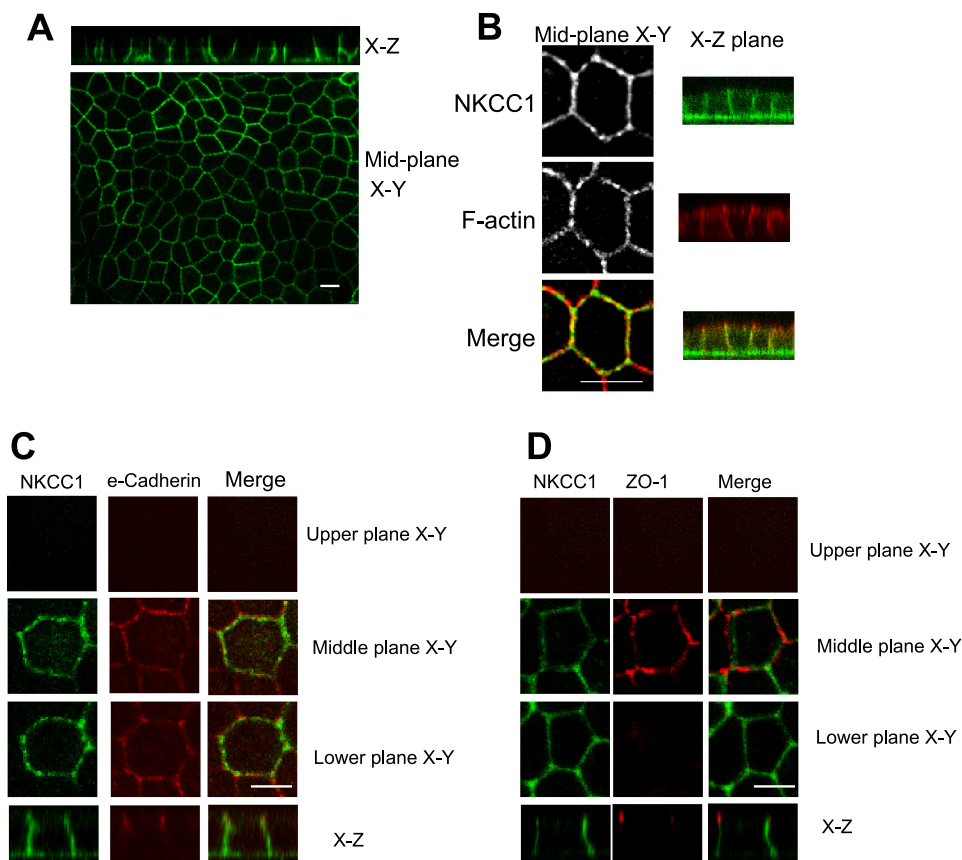


Fig. 2. Immunolocalization of EGFP-NKCC1 in polarized MDCK cells. EGFP-NKCC1 MDCK cells were cultured on Transwell inserts and allowed to develop a polarized epithelium for 4–5 days. Cells were fixed in paraformaldehyde (A) or in cold methanol (B–D) and mounted for confocal microscopy. Cells were labeled with rabbit Alexa Fluor 488-conjugated anti-green fluorescent protein (GFP; 1:200 dilution) to intensify the fluorescent signal (green, A–D). In B–D, cells were double-labeled with rabbit anti-EGFP and Alexa Fluor 594-conjugated phalloidin to label F-actin (B) and mouse anti-E-cadherin (1:200 dilution; C) or with mouse anti-ZO-1 (1:200 dilution; D), followed by an anti-Alexa Fluor 594-conjugated (1:200 dilution) secondary antibody (red, C and D). Upper plane, area above the tight junction; middle plane, area $\sim 2 \mu\text{m}$ below the tight junction; lower plane, area 2–3 μm above the basement membrane. Scale bars, 10 μm .

further characterized NKCC1 localization by using other well-defined membrane markers. We found that EGFP-NKCC1 partially overlaps with E-cadherin on the lateral surface (Fig. 2C) and that NKCC1 staining is restricted to the basolateral membrane, inasmuch as no fluorescence signal was found above ZO-1, a tight junction marker (Fig. 2D). These results demonstrate that EGFP-NKCC1 is appropriately targeted in MDCK cells.

PMA Induces EGFP-NKCC1 Internalization in MDCK Cells

We verified that PMA induces time-dependent internalization of EGFP-NKCC1 in MDCK cells, as previously observed in T84 cells (8, 46). EGFP-NKCC1 MDCK cells were subjected to 100 nM PMA (a concentration that causes a maximal effect; Fig. 1) or DMSO (vehicle) for 0, 2.5, 5, 7.5, 10, and 15 min and then fixed with cold methanol and processed for immunostaining (Fig. 3A). At *time 0*, in the presence or absence of PMA, EGFP-NKCC1 staining localized to the cell periphery, as demarcated by phalloidin staining of F-actin. At this stage of the experiment, NKCC1 and F-actin staining appeared somewhat discontinuous on the lateral membrane, representing real differential distributions along the membrane or apparent differences caused by optical projection of membrane infoldings. After 2.5 min of PMA exposure, EGFP-NKCC1 staining showed a greater discontinuity at the lateral membrane, along with the first appearance of small vesicles in the cytoplasm; at the same time, F-actin staining remained unchanged. From 5 to 7.5 min after PMA stimulation, the fluorescent signal from NKCC1 along the lateral surface largely disappeared, while

the number and size of fluorescent vesicles increased (Fig. 3A). After 10 min, essentially most of the NKCC1 signal was present in relatively large vesicles still arrayed near the lateral membrane, and by 15 min, most of these vesicles had moved and coalesced in the interior of the cell. Throughout this process, F-actin remained strictly localized along the lateral surface of the cell. In cells incubated with DMSO alone for the same amount of time, no changes in NKCC1 localization were observed (Fig. 3B).

To quantify the process of internalization, the number of vesicles (independent of size) within the entire volume of the cell (see MATERIALS AND METHODS) was counted after PMA exposure. It was apparent that PMA induces a ~ 2.2 -fold increase in the number of vesicles over the first 2.5 min, with the number of vesicles reaching a plateau of 18 ± 0.5 and 19.4 ± 0.4 vesicles per cell after 5 and 7.5 min, respectively (Fig. 3C). After 10–15 min of incubation with PMA, the number of vesicles appears to slightly decrease ($n = 6$ experiments, 80 cells). These results suggest that most NKCC1 is endocytosed shortly after stimulation of the cells with PMA, with the number of vesicles reaching an apparent steady state by ~ 5 –7.5 min. The observed decline, although slight, might represent the coalescence of some smaller vesicles into larger vesicles as incubation is continued. Using surface membrane biotinylation, we showed previously that, after 1 h of PMA stimulation, NKCC1 surface expression in T84 cells decreased by $\sim 50\%$ (8). To confirm similar behavior in the MDCK cell model, we exposed EGFP-NKCC1 MDCK to 100 nM PMA for 15 and 30 min. The basolateral side was exposed to biotin for 15 min and washed

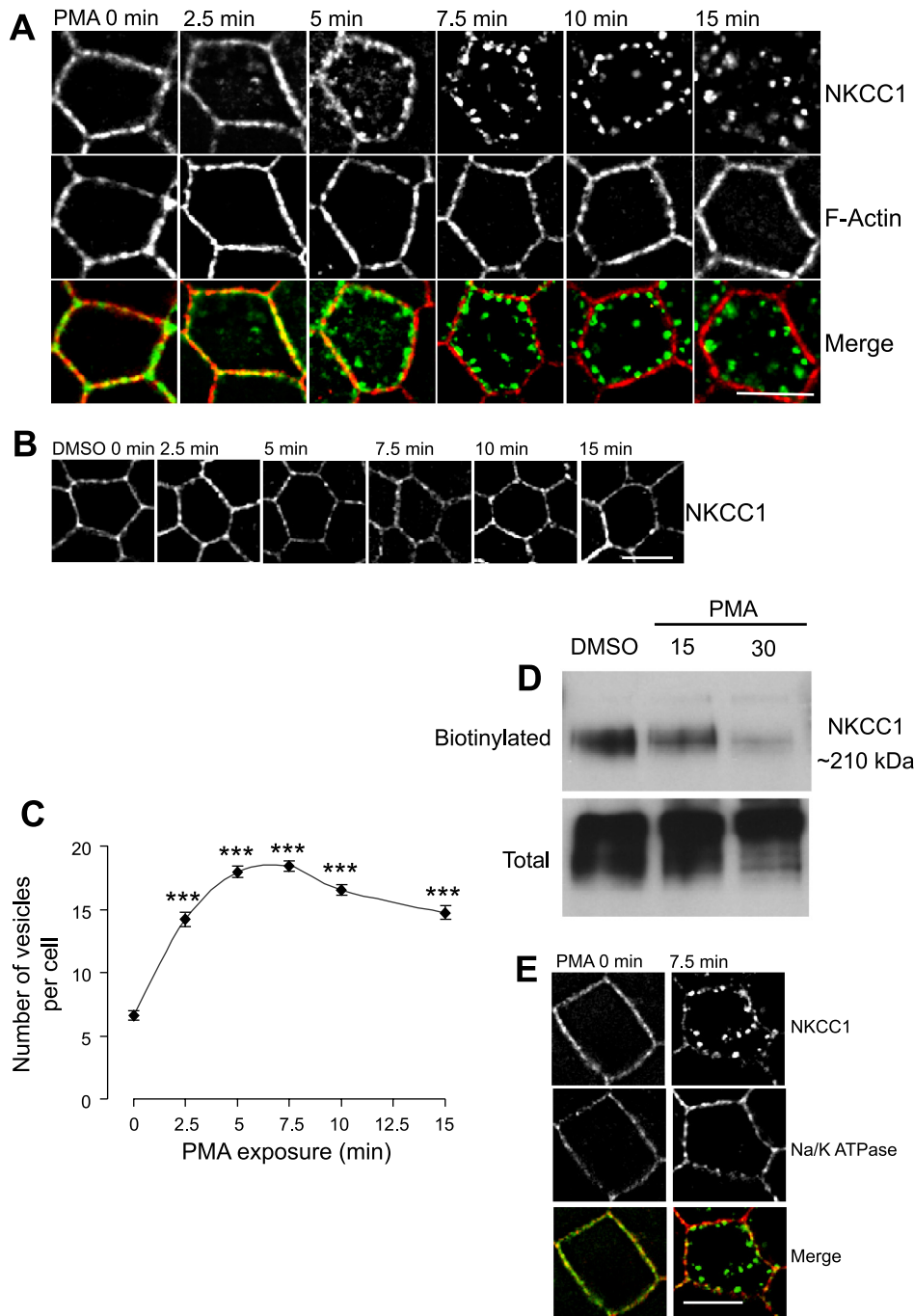


Fig. 3. Effect of PMA on EGFP-NKCC1 and $\text{Na}^+\text{-K}^+\text{-ATPase}$ localization in MDCK cells. Cells were cultured as described in Fig. 2 legend and exposed to 100 nM PMA or vehicle (DMSO) for 0–15 min. *A*: time course. Cells were fixed in cold methanol, labeled with rabbit Alexa Fluor 488-conjugated anti-GFP (1:200 dilution; *A* and *B*) and Alexa Fluor 594-conjugated phalloidin to stain F-actin and then mounted for fluorescence microscopy. *B*: negative control. MDCK cells were exposed to vehicle (DMSO) for 0–15 min. *C*: number of vesicles at each time point in *A* ($n = 4$ experiments, 80 cells). $***P < 0.001$ vs. *time 0* (unpaired *t*-test). *D*: NKCC1 membrane surface biotinylation. After 15 or 30 min of PMA exposure, the basolateral membrane was exposed to sulfo-NHS-biotin. Cells were lysed, and biotinylated proteins were recovered by streptavidin-agarose beads and subjected to Western blotting. NKCC1 proteins were visualized with T4, a mouse anti-NKCC1 antibody (1:1,000 dilution). *E*: effect of PMA on $\text{Na}^+\text{-K}^+\text{-ATPase}$. Cells were treated with vehicle or PMA for 0 or 7.5 min and processed as described above for NKCC1 staining. A mouse anti- α -subunit (1:200 dilution) was used against $\text{Na}^+\text{-K}^+\text{-ATPase}$, followed by Alexa Fluor 594-conjugated antibody (red, 1:200 dilution) to stain $\text{Na}^+\text{-K}^+\text{-ATPase}$. Scale bars, 10 μm .

several times. The cells were lysed, and biotinylated proteins were isolated by incubation with streptavidin-agarose beads and then immunoblotted with an anti-NKCC1 antibody. As shown in Fig. 3D, 15 min of PMA exposure caused a 9.5% decrease in the band intensity compared with control ($n = 2$). After 30 min, EGFP-NKCC1 surface expression decreased by 37.4% (band intensity compared to control, data were normalized to the total cell lysate by densitometry analysis, $n = 2$). The biotinylation values show a lower decrease of NKCC1 than the fluorescence data. We tested if the endogenous NKCC1 (which represents ~25% of the total NKCC1, assayed by Western blot) has a different pattern of internalization during PMA stimulation. We found that the EGFP fluorescent

signal colocalized with the one obtained with an antibody (T4) against NKCC1 (detecting both endogenous and exogenous NKCC1, data not shown). Thus both endogenous and exogenous NKCC1 have a similar internalization pathway, but the endogenous may have a slower rate of internalization, which would explain the difference. On the other hand previous work showed that endogenous NKCC1 functional activity was identical to the human NKCC1 exogenously express in MDCK (41a). It is worth saying that it is difficult to compare the fluorescent data representing the completeness of an event at a particular optical plan, whereas biotinylation is reporting what is happening at the surface level of the whole basolateral membrane.

We investigated whether the effect of PMA was specific to NKCC1 or another basolateral transporter could also be internalized. Toward this end, we determined whether endogenous $\text{Na}^+\text{-K}^+\text{-ATPase}$ was endocytosed during PMA exposure. In the absence of treatment, NKCC1 and the $\text{Na}^+\text{-K}^+\text{-ATPase}$ localized to the lateral membrane of the cell (Fig. 3E). After 7.5 min of pretreatment with 100 nM PMA, we observed redistribution of the EGFP-NKCC1 signal into endocytic vesicles but no endocytosis of the $\text{Na}^+\text{-K}^+\text{-ATPase}$ (Fig. 3E). These results suggest that PKC activation by PMA causes endocytosis of specific, but not generalized, endocytosis of basolateral proteins.

To visualize PMA-stimulated EGFP-NKCC1 internalization in real time, we used time-lapse imaging. Before imaging, we treated EGFP-NKCC1 MDCK cells with 5 mM sodium butyrate for 8 h to augment the transgenic expression of the EGFP-NKCC1 (45). Next, we transferred the cells to complete culture medium without sodium butyrate for 4 h. Before recording the images, we moved the cells to a Hanks' balanced saline solution containing 15 mM HEPES, pH 7.40, for 45 min at 37°C. At *time 0*, we exposed the cells to 100 nM PMA. Then we recorded *z* stacks (0.25 μm) of the entire height of the cells at 1-min intervals. Similarly, we recorded images from cells exposed to vehicle (DMSO) as a control (not shown). We observed a stippling of the lateral surface and loss of surface signal, consistent with NKCC1 internalization within 3 min of PMA exposure (white arrows in Fig. 4; also see supplemental Fig. 10 in the online version of this article). At later time points (3–5 min), analysis of *xz* reconstruction demonstrated invaginations from the basolateral membrane. We observed that the number of membrane buds increased and became isolated vesicles detached from the lateral membrane as time progressed. The vesicles then migrated away from the membrane toward the inside of the cell and appear to be trapped in a lateral region of the cells (>6 min). We also noticed that the number of vesicles decreased with time, giving rise to brighter and apparently larger vesicles, which may have resulted from the fusion of multiple single vesicles (8–14 min) into an endosomal structure, as noted in the previous experiment. We

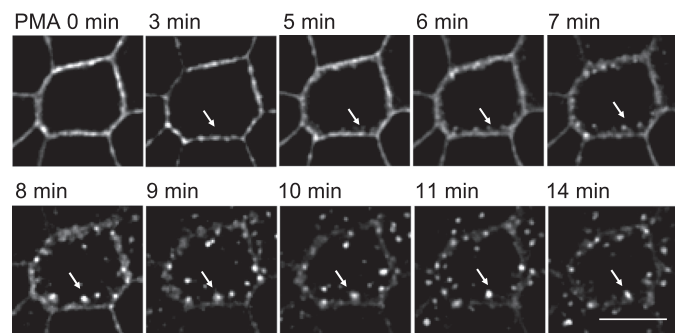


Fig. 4. Time-lapse imaging of EGFP-NKCC1 in MDCK cells during PMA exposure. Cells were cultured as described in Fig. 2 legend. Before imaging, EGFP-NKCC1 MDCK cells were treated with 5 mM sodium butyrate for 8 h to augment transgenic expression of EGFP; then cells were transferred to complete culture medium without sodium butyrate for 4 h. Before live imaging, cells were transferred to a Hanks' balanced saline solution and mounted on a temperature-controlled microscope stage for 45 min. Images were acquired every minute and processed for morphometric analysis. White arrows show the fate of 1 specific endocytic vesicle as it progresses into the endocytic pathway; therefore, the focal plane was changed to track the vesicle with time. Scale bar, 10 μm .

did not characterize the fate of the vesicles (recycling vs. degradation), nor did we determine the type of intracellular compartments in which NKCC1 fluorescence accumulates.

Mapping of NKCC1 Internalization Pathway

PMA-induced EGFP-NKCC1 endocytosis does not induce actin reorganization. Macropinocytosis is accompanied by major rearrangements of cortical actin, such as the actin-driven formation of membrane protrusions (5, 40). To test the effect of PMA on actin rearrangement in MDCK cells, phalloidin coupled to Alexa Fluor 594 was used to stain filamentous actin. As shown in Fig. 3A, we did not observe actin rearrangement or colocalization of EGFP-NKCC1 with actin during PMA-induced NKCC1 endocytosis. Thus NKCC1 internalization is probably not associated with macropinocytosis during PMA treatment.

Dynamin is involved in PMA-induced EGFP-NKCC1 endocytosis. Dynamin, a GTPase involved in pinching off endocytic vesicles from the membrane, is an important component of vesicle formation in clathrin- and caveolin-mediated pathways (5, 31). To test the involvement of dynamin in NKCC1 internalization, we utilized an antibody against dynamin II, a ubiquitous isoform of the dynamin family, to stain PMA-treated cells. Western blotting of MDCK whole cell lysate showed that the dynamin II antibody recognized a single band and was suitable for immunocytochemistry (Fig. 5A).

Cells were cultured as described in MATERIALS AND METHODS and fixed with cold methanol. In the absence of PMA stimulation, dynamin showed a punctate staining at the cell membrane and discrete staining inside the cell (Fig. 5B). At *time 0*, the merge images show that the colocalization of EGFP-NKCC1 and dynamin II is at the membrane and present a discontinuous pattern. PMA exposure caused a redistribution of dynamin II: at 5 min there was an apparent increase of the dynamin staining, and the signal became concentrated into large punctate vesicles as time progressed; the dynamin II pattern staining into larger vesicles appeared to be associated with PMA treatment, because in control cells we did not see such staining (Fig. 5B). We quantified the amount of EGFP-NKCC1 signal that colocalized with dynamin II (Fig. 5C). We found that $39 \pm 2.2\%$ ($n = 5$, number of cells 70) of EGFP-NKCC1 staining colocalized with dynamin II at *time 0*. Subsequently, at 7.5 min there is $58 \pm 1.6\%$ ($n = 5$) colocalization and at 10 min it reaches $73 \pm 1.7\%$ ($n = 5$). These results indicate that EGFP-NKCC1 internalization is partially associated with dynamin II. At 7.5 and 10 min, colocalization of dynamin with EGFP-NKCC1 was in larger vesicular structures, as indicated by the arrows after PMA stimulation. It may represent dynamin-associated vesicles leaving or merging with an endosome, inasmuch as dynamin has previously been shown to be involved in vesicular trafficking (23, 38).

EGFP-NKCC1 endocytosis is associated with clathrin. The previous results show the participation of dynamin II in NKCC1 internalization. We first tested the involvement of clathrin, because dynamin II participates in the clathrin and caveolin internalization pathway. As shown in Fig. 6A, in MDCK total cell lysate, the clathrin antibody recognized one specific band at ~ 190 kDa, the expected size of clathrin heavy chain.

Exposure of the cells to PMA induced membrane invaginations at the early time points followed by a progressive formation of vesicles and disappearance of EGFP-NKCC1 signal

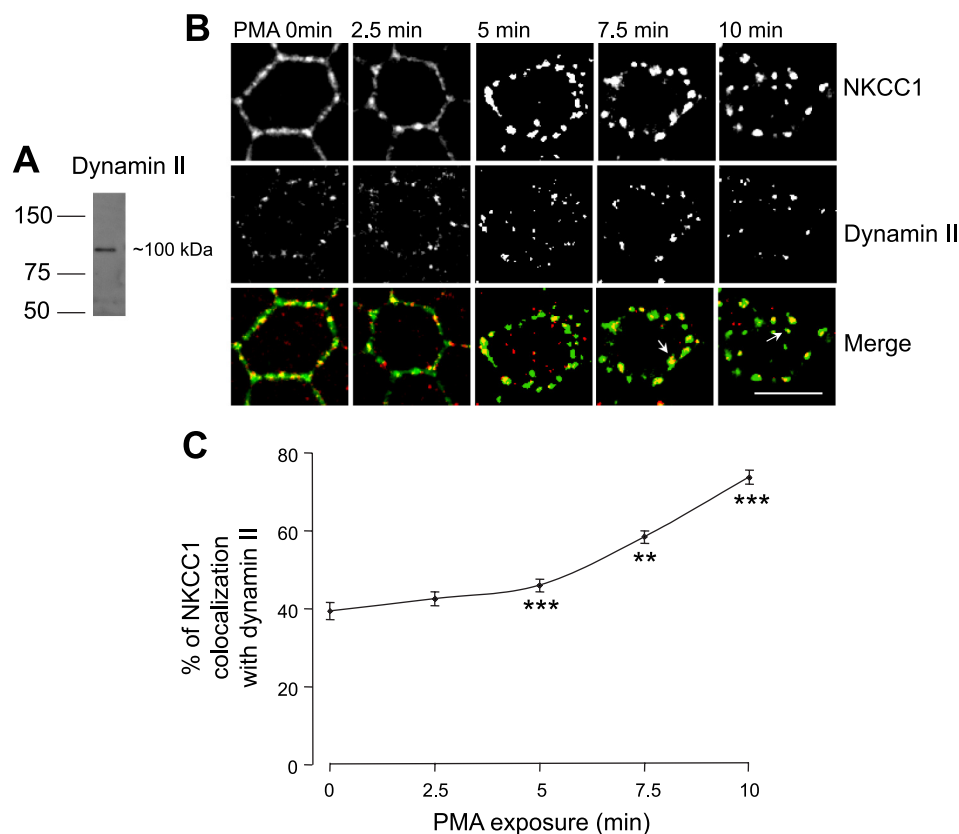


Fig. 5. Involvement of dynamin in PMA-induced EGFP-NKCC1 endocytosis. *A*: Western blot of whole MDCK cell lysate probed for dynamin II using a rabbit anti-dynamin antibody at 1:200 dilution. Cells were cultured as described in Fig. 2 legend. *B*: colocalization of EGFP-NKCC1 with dynamin. Cells were cultured as described in Fig. 2 legend and exposed to 100 nM PMA for 0–10 min. Cells were double-labeled with mouse Alexa Fluor 488-conjugated anti-GFP (green) and anti-dynamin II (1:200 dilution). White arrows show NKCC1 colocalization with dynamin II in large vesicular structures at late time points and nonrecycling of dynamin II to the membrane during PMA stimulation. Scale bar, 10 μ m. *C*: percentage of NKCC1 colocalization with dynamin II in large vesicular structures colocalizing with dynamin II staining calculated for each time point of *B* ($n = 4$ experiments, 60 cells). ** $P < 0.01$; *** $P < 0.001$ vs. *time 0* (unpaired *t*-test).

at the membrane surface (Fig. 6B). After 5 min of PMA exposure, the vesicles coalesced, and at 10 min fewer vesicles were visible. In untreated EGFP-NKCC1 MDCK cells, clathrin localized predominantly to the plasma membrane in a granular, punctate pattern, as previously reported (9), and some dotted staining in the cytosol was also visible. After PMA stimulation, the clathrin heavy chain staining appeared more vesicular. When the EGFP-NKCC1 and clathrin fluorescence signals were merged, the majority of the EGFP-NKCC1 vesicles colocalized with clathrin at 2.5 and 5 min. As described previously for dynamin II, the colocalization of clathrin and NKCC1 can be seen in a large vesicular structure at 7.5 min (see arrow in Fig. 6A). Again, this punctuated colocalization in larger structures may represent clathrin-associated vesicles merging with or leaving endosome-like structures, as previously shown by others (7). Nevertheless, the increase of clathrin staining in those larger vesicular-type structures is specific to PMA stimulation; interestingly, clathrin during PMA stimulation does not return to the plasma membrane, rather, it remains sequestered in the larger vesicular compartments.

In Fig. 6C, we quantified the number of NKCC1 vesicles that colocalized with clathrin staining. In order for a vesicle to be considered positive for colocalization, the fluorescence signal of both channels (green for EGFP and red for clathrin) had to overlap in at least two optical sections. In control monolayers (PMA at *time 0*), $41 \pm 2.8\%$ ($n = 4$ experiments, 100 cells) of NKCC1 staining colocalized with clathrin. After 2.5 min of treatment with PMA, $80 \pm 2\%$ of EGFP-NKCC1 vesicles colocalized with clathrin. These data strongly suggest that PMA-induced NKCC1 endocytosis is associated with the clathrin pathway.

The TfR is known to be internalized through clathrin-coated vesicles (40), and it is often used as a marker of this pathway (7, 51, 52). EGFP-NKCC1 MDCK cells were treated with PMA, fixed in methanol, and costained for NKCC1 and the TfR. As shown in Fig. 6D, in the absence of PMA, NKCC1 staining is at the lateral surface, whereas TfR staining is punctate, with a cytosolic distribution, probably because the TfR undergoes constitutive endocytosis, as reported by others (49). After PMA stimulation, we observed an increase of TfR endocytosis, as previously reported (10), and almost all NKCC1 signal colocalized with the TfR, strongly supporting our previous result that NKCC1 endocytosis is associated with clathrin.

NKCC1 endocytosis is not associated with caveolin 1. Caveolin-mediated endocytosis is another pathway for the internalization of proteins (5, 40). A recent study showed that NKCC2, the absorptive $\text{Na}^+\text{-K}^+\text{-Cl}^-$ cotransporter isoform, is associated with lipid rafts in caveolae during vasopressin-induced NKCC2 trafficking (50). We investigated whether NKCC1 may also associate with the caveolae during PMA exposure. We used caveolin as a marker of the caveolae-mediated endocytosis (40). As shown on the Western blot, the anti-caveolin antibody recognized one band at ~ 25 kDa, the expected size for caveolin (Fig. 7A). Cells were cultured and fixed as described in Fig. 2. Exposure of EGFP-NKCC1 MDCK cells to PMA caused NKCC1 endocytosis and a redistribution of caveolin 1 (Fig. 7B). Nevertheless, when we merged the images, we found that the extent of NKCC1 colocalization with caveolin was only 12% at 2.5 min and reached a maximum of 14% at 7.5 min ($n = 4$ experiments, 60

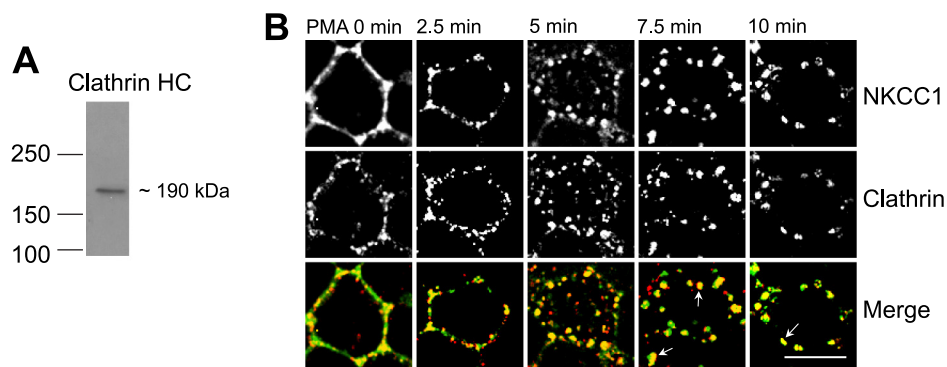
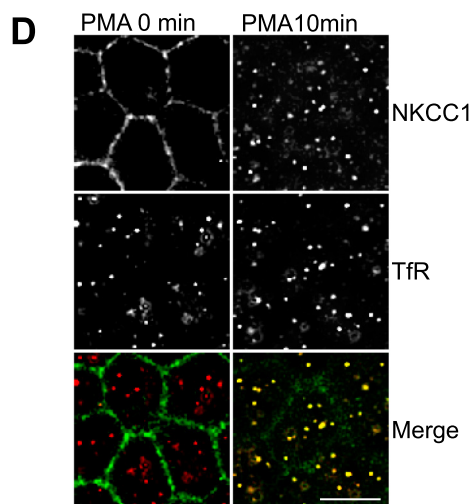
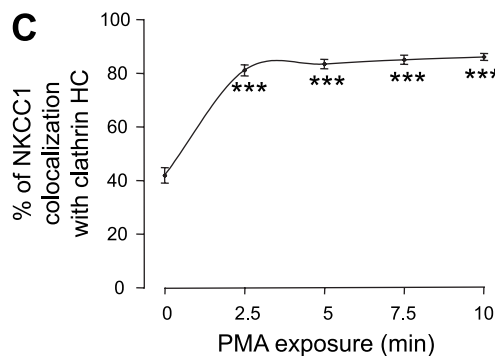


Fig. 6. Colocalization of EGFP-NKCC1 vesicles with clathrin and the transferrin receptor (TfR) during PMA exposure. **A:** Western blot of whole MDCK cell lysate probed for clathrin using a rabbit anti-clathrin heavy chain (HC) antibody (1:200 dilution). Cells were cultured as described in Fig. 2 legend. **B:** colocalization of EGFP-NKCC1 with clathrin. Cells were cultured as described in Fig. 2 legend and exposed to 100 nM PMA for 0–10 min. Cells were double-labeled with rabbit Alexa Fluor 488-conjugated anti-GFP (green, 1:200 dilution) and rabbit anti-clathrin (1:200 dilution). Alexa Fluor 594-conjugated secondary antibody (red, 1:200 dilution) was used to visualize clathrin. Arrows show NKCC1 colocalization with clathrin in large vesicular structures at late time points and nonrecycling of clathrin to the membrane during PMA stimulation. Scale bar, 10 μ m. **C:** percentage of NKCC1 vesicles colocalizing with clathrin staining calculated for each time point of **B** ($n = 4$ experiments, 90 cells). *** $P < 0.001$ vs. *time 0* (unpaired *t*-test). **D:** colocalization of NKCC1 with the TfR. Cells were cultured as described in Fig. 2 legend and exposed to 100 nM PMA for 10 min. Cells were double-labeled with rabbit Alexa Fluor 488-conjugated anti-GFP (green, 1:200 dilution) and rabbit CD71 anti-TfR (1:200 dilution). Alexa Fluor 594-conjugated secondary antibody (red, 1:200 dilution) was used to visualize the TfR. Scale bar, 10 μ m.



cells), suggesting that caveolin-dependent endocytosis does not represent the major pathway of EGFP-NKCC1 internalization.

Effect of Endocytosis Blockers on PMA-Induced NKCC1 Internalization

Chlorpromazine, an inhibitor of clathrin-mediated endocytosis, blocks PMA-induced EGFP-NKCC1 internalization. Our previous results suggest that PMA-induced EGFP-NKCC1 endocytosis occurs predominantly via the clathrin-mediated pathway. To verify our results, we used a pharmacological approach to block the different pathways tested above. We used chlorpromazine, methyl- β -cyclodextrin, and amiloride to block the clathrin-, caveolin-, and macropinocytosis-mediated pathways, respectively (21). Pretreatment of the EGFP-NKCC1 MDCK cells with 100 μ M chlorpromazine blocked PMA-

induced NKCC1 endocytosis compared with control (Fig. 8A). On the other hand, neither 10 mM methyl- β -cyclodextrin nor 5 mM amiloride prevented PMA-induced NKCC1 endocytosis (Fig. 8A, third and fourth rows).

We quantified the effect of each inhibitor on PMA-induced NKCC1 endocytosis and, as shown in Fig. 8B, found that 100 μ M chlorpromazine caused a substantial inhibition of 23, 61, 62, 55, and 47% ($P < 0.001$, unpaired *t*-test for each point, $n = 6$ experiments, 80 cells) at *time 0* and 2.5, 5, 7.5, and 10 min, respectively, compared with control. Amiloride (5 mM) did not cause a significant inhibition, except at 5 min, when we observed a 14% inhibition ($P < 0.05$, unpaired *t*-test).

The dynamin inhibitor dynasore blocks PMA-induced EGFP-NKCC1 endocytosis. Dynasore is a cell-permeant inhibitor of dynamin GTPase identified in a compound screening (30). We

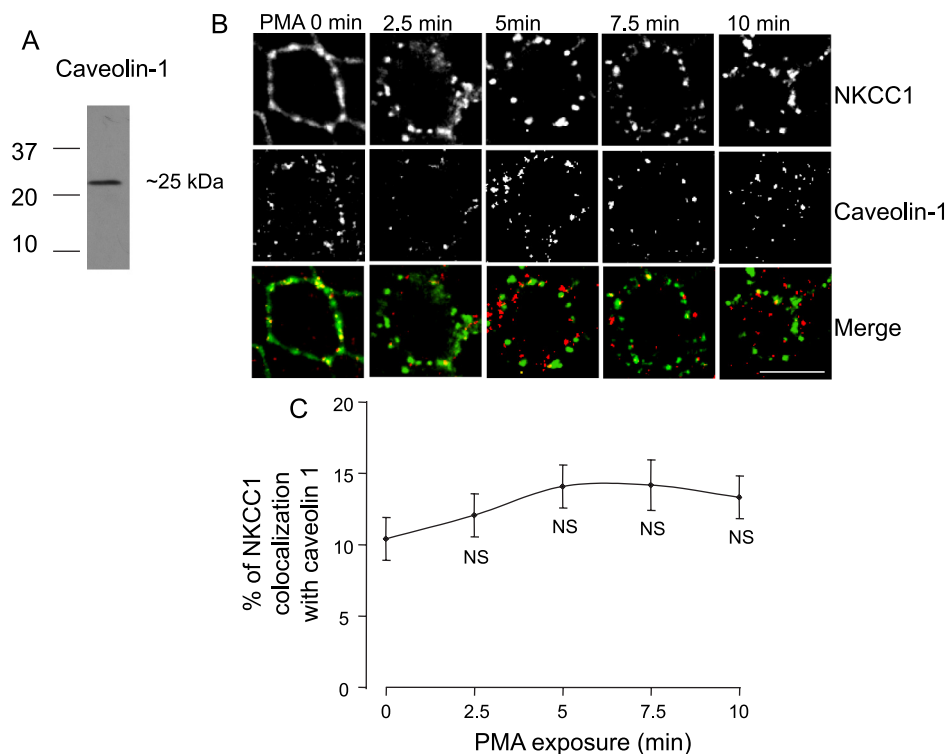


Fig. 7. NKCC1 endocytosis is not associated with caveolin. Cells were cultured as described in Fig. 2 legend. **A**: Western blot of whole MDCK cell lysate probed for caveolin-1 using a rabbit anti-caveolin-1 antibody (1:200 dilution). **B**: cells were cultured as described in Fig. 2 legend and then exposed to 100 nM PMA for 0–10 min. Cells were double-labeled with mouse Alexa Fluor 488-conjugated anti-GFP (green, 1:200 dilution) and anti-caveolin-1 (1:200 dilution). Alexa Fluor 594-conjugated secondary antibody (red, 1:200 dilution) was used to visualize caveolin. Scale bar, 10 μ m. **C**: percentage of NKCC1 vesicles colocalizing with caveolin staining calculated for each time point of **B** ($n = 4$ experiments, 60 cells). NS, not significantly different from *time 0* (unpaired *t*-test).

tested its ability to block PMA-induced EGFP-NKCC1 endocytosis and, as shown in Fig. 9A, found that pretreatment of the cells with 80 μ M dynasore inhibited PMA-induced NKCC1 internalization.

Quantification of the dynasore effect (Fig. 9B) showed that dynasore blocked PMA-induced EGFP-NKCC1 endocytosis by 37 and 28% at *time 0* and 2.5 min, respectively ($P < 0.001$, unpaired *t*-test, $n = 5$ experiments, 60 cells). Dynasore blocked EGFP-NKCC1 endocytosis by ~41, 42, and 36% at 5, 7.5, and 10 min, respectively ($P < 0.001$, unpaired *t*-test, $n = 5$ experiments, 60 cells). These results demonstrate that dynamin is at least partially involved in the endocytic pathway and are consistent with the significant involvement of the clathrin-mediated pathway in PMA-stimulated NKCC1 endocytosis.

DISCUSSION

Lessons from genetic diseases have demonstrated the importance of studying the regulation of the membrane surface expression of ion transporters, in addition to the specific regulation of their ion transport capability. For instance, there are membrane trafficking defects in cystic fibrosis ($\Delta 508$ CFTR), Liddle's syndrome (mutation of the epithelial Na^+ channel), and aquaporin-2 trafficking in X-linked nephrogenic diabetes insipidus associated with mutation of the vasopressin receptor (3, 4, 41). NKCC1, an important Cl^- regulatory component, may be involved in diseases of Cl^- transport. Therefore, the aim of our study was to investigate the internalization pathways of NKCC1 during PKC activation by PMA to better understand this aspect of the physiological regulation of the transporter.

Epithelial Cl^- secretion is the fundamental means of mucosal surface hydration that serves to lubricate the lining of the

gut and other epithelial interfaces with the external environment. Dysregulation of Cl^- secretion accounts for the diarrheal response that accompanies a number of inflammatory and infectious enteropathies (13, 34). Classically, the major regulatory site for Cl^- secretion was envisioned at the level of apical Cl^- channels such as CFTR. However, it has become increasingly clear that the basolateral NKCC1 transporter is a critical independent locus for controlling transepithelial secretion (19, 34).

In native colonic crypts and the model T84 cell line, the muscarinic agonist carbachol, acting via PKC activation, downregulates NKCC1 membrane surface expression (8, 43). In T84 cells, we have extensively characterized the functional inhibition of NKCC1 induced by the diacylglycerol mimetic PMA. Early inhibition of NKCC1 activity by PMA correlates with a reduction in the number of binding sites for radiolabeled bumetanide and endocytosis of NKCC1 (8, 11, 35, 37).

The T84 cell line represents an excellent cell model to study Cl^- secretion and its regulation, but it is ill-suited for expression of exogenous protein and definition of trafficking events. Thus we used the MDCK cell; when stably expressed in MDCK cells, EGFP-NKCC1 retained basolateral targeting, as demonstrated in Fig. 2. It is expressed below the tight junction, overlaps E-cadherin, and displays the same distribution pattern as the endogenous basolateral $\text{Na}^+\text{-K}^+\text{-ATPase}$ (Fig. 3E). Collectively, these results show that exogenous NKCC1 is normally distributed in MDCK cells. PMA caused a dose- and time-dependent NKCC1 endocytosis in MDCK cells, as previously observed in T84 cells (11, 46), demonstrating that our cell system is valid to investigate the internalization pathway of NKCC1 during PMA exposure.

Among the three pathways we investigated (clathrin- and caveolin-mediated endocytosis and macropinocytosis), our ex-

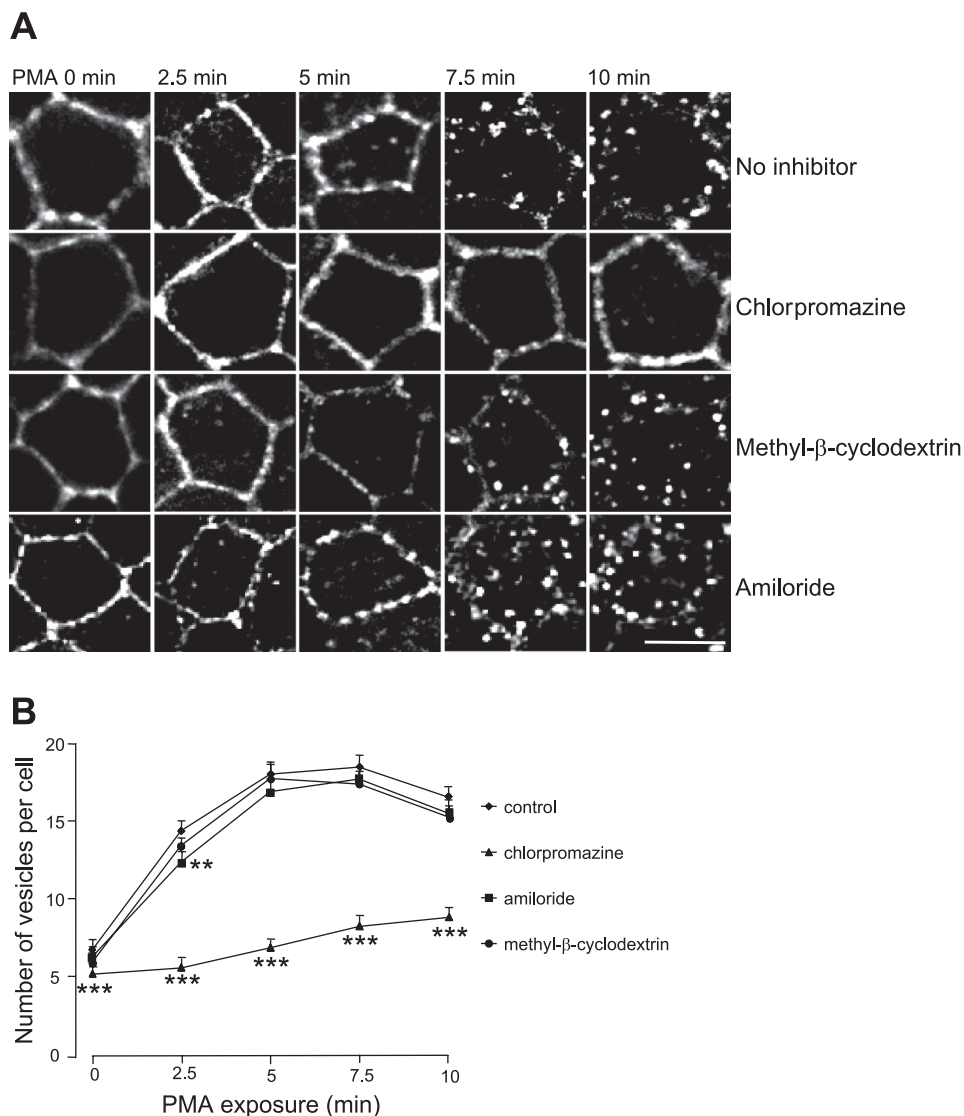


Fig. 8. Effect of chlorpromazine, methyl-β-cyclodextrin, and amiloride on PMA-induced EGFP-NKCC1 endocytosis. *A*: effect of endocytic inhibitors on PMA-induced NKCC1 endocytosis. Cells were cultured and stained as described in Fig. 2 legend, preincubated for 30 min with vehicle (no inhibitor) or in the presence of 100 μM chlorpromazine, 10 mM methyl-β-cyclodextrin, or 5 mM amiloride, and then exposed to PMA for 0–10 min. Scale bar, 10 μm. *B*: effect of endocytic inhibitors on the number of endocytic vesicles for each time point of *A* ($n = 6$ experiments, 80 cells). ** $P < 0.01$; *** $P < 0.001$ (unpaired *t*-test).

periments indicate that the dominant pathway for NKCC1 internalization involves clathrin. Evidence for the clathrin-associated pathway is based on immunocytochemistry and pharmacological experiments.

We found that ~80% of the EGFP-NKCC1 colocalized with clathrin and ~40% with dynamin II during the shortest PMA exposure. The lower percentage of colocalization of NKCC1 with dynamin II may be attributed to the fact that dynamin II is not solely involved in clathrin-mediated endocytosis, but it is also involved in the caveolin-mediated endocytosis (5). Therefore, only a certain fraction of dynamin II is probably associated with clathrin. As the PMA stimulation persists, it may lead to a recruitment of dynamin II to the clathrin vesicles, explaining the progressive increase of colocalization of NKCC1 with dynamin II in Fig. 5*B*. In our experiments, we focused on studying the internalization pathway at early time points, because we were mostly interested in mapping the entry mechanism. Other groups demonstrated that clathrin is also involved in trafficking of newly synthesized proteins and membrane recycling and is, therefore, not solely expressed at the membrane (7). Consequently, observation of colocalization

at the late time point may only reflect the involvement of clathrin in directing the vesicles to a recycling or degradative pathway. The same is true for dynamin II, which plays a role in the trafficking of the vesicles at the trans-Golgi network and other organelles such as endosomes (23, 38). Interestingly, we observed that, during PMA exposure, clathrin and dynamin II staining accumulated in large structures, with no recovery of their staining at the plasma membrane. It appears that, in the continuous presence of PMA, neither clathrin nor dynamin II recycled back to the membrane. PMA may somehow cause retention of dynamin II and clathrin into endosome-like structures in MDCK cells.

To further confirm our observation that NKCC1 internalization is associated with clathrin, we used the TfR as a positive marker of the clathrin pathway. In these experiments, we observed that almost all EGFP-NKCC1 colocalized with the TfR (Fig. 6*D*). On the other hand, we found minimal colocalization of EGFP-NKCC1 with caveolin (Fig. 7) by immunocytochemistry. In that respect, it appears that the trafficking pattern of NKCC1 is different from that of NKCC2, which is found in lipid rafts during vasopressin stimulation (50).

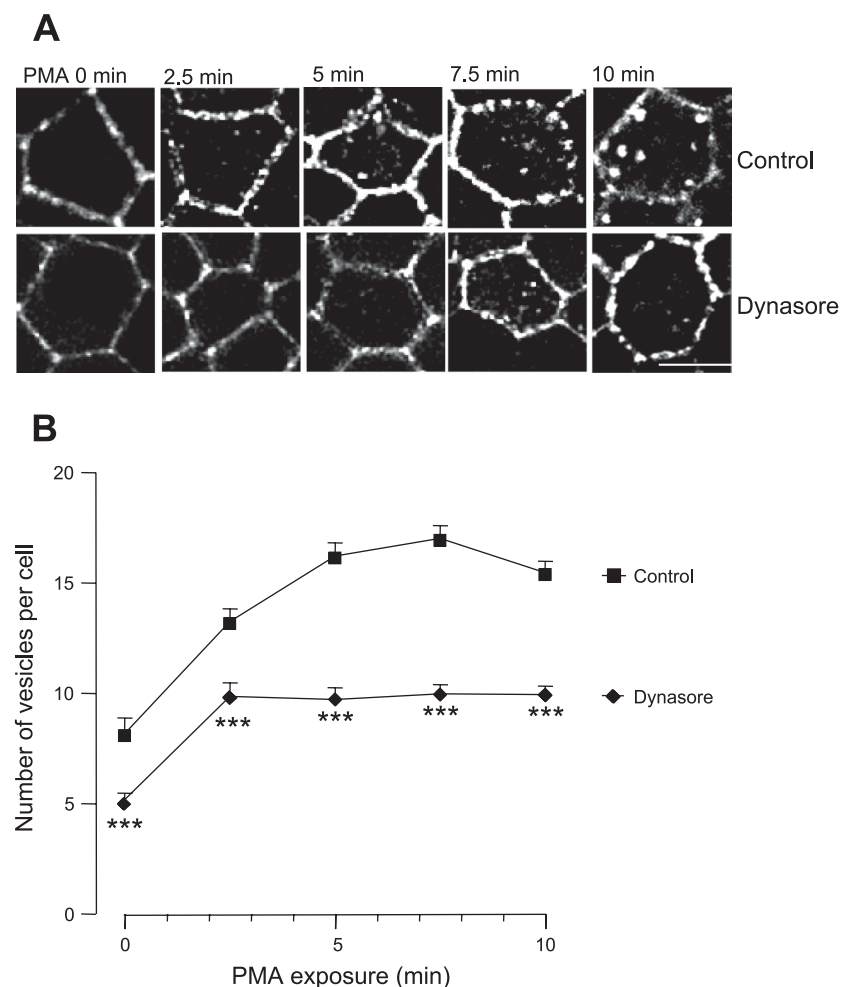


Fig. 9. Dynasore blocks PMA-induced EGFP-NKCC1 endocytosis. Cells were cultured and stained as described in Fig. 2 legend. *A*: cells were preincubated for 30 min with vehicle (control) or in presence of 80 μ M dynasore. *B*: number of EGFP-NKCC1 vesicles per cell for each time point in *A* in the presence or absence of dynasore ($n = 5$ experiments, 60 cells). *** $P < 0.001$ (unpaired t -test).

The second piece of evidence supporting the clathrin-associated pathway is the pharmacological profile. Chlorpromazine, a blocker of clathrin-mediated endocytosis (48), blocked substantially (~60%) NKCC1 endocytosis during the first 5 min. Dynasore, a blocker of dynamin II (30), also produced a significant blockade (~40%) of NKCC1 endocytosis evoked by PMA. Chlorpromazine has proved to be a potent inhibitor of clathrin-mediated endocytosis. Only two studies reported chlorpromazine as a blocker of phagocytosis in immune cells (21). To the best of our knowledge, dynasore has not been reported to interfere with phagocytosis or macropinocytosis. Therefore, the pharmacological selectivity of the two inhibitors also supports the clathrin pathway. Furthermore, neither methyl- β -cyclodextrin nor amiloride, which inhibit the caveolin-dependent and macropinocytosis pathways, respectively, blocked PMA-induced NKCC1 endocytosis (Fig. 8B). The lack of effect of amiloride and the nonrearrangement of actin do not support the involvement of macropinocytosis. Collectively, these results strongly suggest that NKCC1 endocytosis during PMA exposure is associated with clathrin.

In the absence of a stimulus, the K^+ channel Kir2.3, the human organic ion transporter, and the dopamine transporter undergo constitutive endocytosis (20, 32, 52). In our experiments, in the absence of PMA stimulation, we also noticed that ~40% of EGFP-NKCC1 colocalized with clathrin and dynamin II, suggesting that, in MDCK cells, NKCC1 may un-

dergo a constitutive endocytosis. Although in the nonstimulated state the majority of NKCC1 staining is at the membrane, we did visualize some punctate staining in the cell. The fate of these vesicles might also be different from the fate of the vesicles retrieved from the membrane during PKC activation, which accumulates NKCC1 in large vesicles, which are easier to visualize. A constitutive endocytosis of NKCC1 remains to be evaluated. In T84 cells, we did not observe constitutive endocytosis of NKCC1 via selective surface biotinylation: this approach may not be sufficiently sensitive to detect this behavior, depending on the baseline rate of internalization. However, in native colonic crypts, NKCC1 staining was evident in vesicular perinuclear structures, and vesicular staining was noted at the basal pole of the cells in the absence of stimulus. This finding suggests the presence of a pool of newly synthesized or constitutively trafficking NKCC1 (43).

Over the past few years, PKC has emerged as a hub in controlling endocytosis of channels, transporters, and receptors (1, 11, 18, 22, 25, 40, 42). Distinct constitutive and PKC-mediated endocytic signals have been identified, for example, in the dopamine transporter (20), but in the case of NKCC1, no PKC phosphorylation sites are present. The link between PKC and NKCC1 remains to be determined. Several groups have shown that membrane proteins such as aquaporin-2 and the dopamine and glutamate transporters are ubiquitinated during PKC activation. The addition of ubiquitin moieties to the

proteins represents a signal for endocytosis (15, 24, 39). The ubiquitination by clathrin coat-associated sorting membrane proteins appears to be a new signal for clathrin-mediated endocytosis (47). Such a signaling cascade remains to be explored for NKCC1.

Our data are the first to address the internalization pathway of NKCC1 during PKC activation in a polarized epithelial cell and demonstrate that PKC activation selectively causes NKCC1 internalization via a clathrin-associated pathway. The fate of the vesicles remains to be explored to distinguish between degradation and recycling. Future experiments are necessary to confirm that, in the intestinal cell line T84 or in the colonic crypt, NKCC1 traffics through the clathrin pathway during PKC activation by physiological agonists such as acetylcholine.

ACKNOWLEDGMENTS

The authors thank the Epithelial Pathobiology Group of the Department of Surgery at the University of Chicago for constructive comments on the manuscript and Dr. Vytas Bindokas for technical help with the fluorescence microscopy and Image J analysis software.

GRANTS

This work was supported by National Institute of Diabetes and Digestive and Kidney Diseases Grant DK-48010 (to J. B. Matthews). L. Shen is a fellow of the Crohn's and Colitis Foundation of America sponsored by Ms. Laura McAteer Hoffman.

DISCLOSURES

No conflicts of interest are declared by the author(s).

REFERENCES

- Alvi F, Idkowiak-Baldys J, Baldys A, Raymond JR, Hannun YA. Regulation of membrane trafficking and endocytosis by protein kinase C: emerging role of the pericentrin, a novel protein kinase C-dependent subset of recycling endosomes. *Cell Mol Life Sci* 64: 263–270, 2007.
- Anderson RG. Caveolae: where incoming and outgoing messengers meet. *Proc Natl Acad Sci USA* 90: 10909–10913, 1993.
- Bertrand CA, Frizzell RA. The role of regulated CFTR trafficking in epithelial secretion. *Am J Physiol Cell Physiol* 285: C1–C18, 2003.
- Brown D. The ins and outs of aquaporin-2 trafficking. *Am J Physiol Renal Physiol* 284: F893–F901, 2003.
- Conner SD, Schmid SL. Regulated portals of entry into the cell. *Nature* 422: 37–44, 2003.
- Darman RB, Flemmer A, Forbush B. Modulation of ion transport by direct targeting of protein phosphatase type 1 to the Na-K-Cl cotransporter. *J Biol Chem* 276: 34359–34362, 2001.
- Deborde S, Perret E, Gravotta D, Deora A, Salvarezza S, Schreiner R, Rodriguez-Boulon E. Clathrin is a key regulator of basolateral polarity. *Nature* 452: 719–723, 2008.
- Del Castillo IC, Fedor-Chaiken M, Song JC, Starlinger V, Yoo J, Matlin KS, Matthews JB. Dynamic regulation of Na⁺-K⁺-2Cl⁻ cotransporter surface expression by PKC-ε in Cl⁻-secretory epithelia. *Am J Physiol Cell Physiol* 289: C1332–C1342, 2005.
- Dell'Angelica EC, Klumperman J, Stoorvogel W, Bonifacio JS. Association of the AP-3 adaptor complex with clathrin. *Science* 280: 431–434, 1998.
- a. Delpire E, Rauchman MI, Beier DR, Hebert SC, Gullans SR. Molecular cloning and chromosome localization of a putative basolateral Na⁺-K⁺-2Cl⁻ cotransporter from mouse inner medullary collecting duct (mIMCD-3) cells. *J Biol Chem* 269: 25677–25683, 1994.
- b. Dowd BF, Forbush B. PASK (proline-alanine-rich STE20-related kinase), a regulatory kinase of the Na-K-Cl cotransporter (NKCC1). *J Biol Chem* 278: 27347–27353, 2003.
- Eichholtz T, Vosseveld P, van Overveld M, Ploegh H. Activation of protein kinase C accelerates internalization of transferrin receptor but not of major histocompatibility complex class I, independent of their phosphorylation status. *J Biol Chem* 267: 22490–22495, 1992.
- Farokhzad OC, Sagar GD, Mun EC, Sicklick JK, Lotz M, Smith JA, Song JC, O'Brien TC, Sharma CP, Kinane TB, Hodin RA, Matthews JB. Protein kinase C activation downregulates the expression and function of the basolateral Na⁺/K⁺/2 Cl⁻ cotransporter. *J Cell Physiol* 181: 489–498, 1999.
- Flagella M, Clarke LL, Miller ML, Erway LC, Giannella RA, Andringa A, Gawenis LR, Kramer J, Duffy JJ, Doetschman T, Lorenz JN, Yamoah EN, Cardell EL, Shull GE. Mice lacking the basolateral Na-K-2Cl cotransporter have impaired epithelial chloride secretion and are profoundly deaf. *J Biol Chem* 274: 26946–26955, 1999.
- Fondacaro JD. Intestinal ion transport and diarrheal disease. *Am J Physiol Gastrointest Liver Physiol* 250: G1–G8, 1986.
- Gagnon KB, England R, Delpire E. Volume sensitivity of cation-Cl⁻ cotransporters is modulated by the interaction of two kinases: Ste20-related proline-alanine-rich kinase and WNK4. *Am J Physiol Cell Physiol* 290: C134–C142, 2006.
- González-González IM, García-Tardón N, Giménez C, Zafra F. PKC-dependent endocytosis of the GLT1 glutamate transporter depends on ubiquitination of lysines located in a C-terminal cluster. *Glia* 56: 963–974, 2008.
- Gottardi CJ, Dunbar LA, Caplan MJ. Biotinylation and assessment of membrane polarity: caveats and methodological concerns. *Am J Physiol Renal Fluid Electrolyte Physiol* 268: F285–F295, 1995.
- Graeve L, Drickamer K, Rodriguez-Boulon E. Polarized endocytosis by Madin-Darby canine kidney cells transfected with functional chicken liver glycoprotein receptor. *J Biol Chem* 109: 2809–2816, 1989.
- Guillet BA, Velly LJ, Canolle B, Masméjean FM, Nieouillon AL, Pisano P. Differential regulation by protein kinases of activity and cell surface expression of glutamate transporters in neuron-enriched cultures. *Neurochem Int* 46: 337–346, 2005.
- Haas M, Forbush B, 3rd. The Na-K-Cl cotransporters. *J Bioenerg Biomembr* 30: 161–172, 1998.
- Holton KL, Loder MK, Melikian HE. Nonclassical, distinct endocytic signals dictate constitutive and PKC-regulated neurotransmitter transporter internalization. *Nat Neurosci* 8: 881–888, 2005.
- Ivanov AI. Pharmacological inhibition of endocytic pathways: is it specific enough to be useful? *Methods Mol Biol* 440: 15–33, 2008.
- Jiao J, Garg V, Yang B, Elton TS, Hu K. Protein kinase C-ε induces caveolin-dependent internalization of vascular adenosine 5'-triphosphate-sensitive K⁺ channels. *Hypertension* 52: 499–506, 2008.
- Jones SM, Howell KE, Henley JR, Cao H, McNiven MA. Role of dynamin in the formation of transport vesicles from the trans-Golgi network. *Science* 279: 573–577, 1998.
- Kamsteeg EJ, Hendriks G, Boone M, Konings IB, Oorschot V, van der Sluijs P, Klumperman J, Deen PM. Short-chain ubiquitination mediates the regulated endocytosis of the aquaporin-2 water channel. *Proc Natl Acad Sci USA* 103: 18344–18349, 2006.
- Ko B, Joshi LM, Cooke LL, Vazquez N, Musch MW, Hebert SC, Gamba G, Hoover RS. Phorbol ester stimulation of RasGRP1 regulates the sodium-chloride cotransporter by a PKC-independent pathway. *Proc Natl Acad Sci USA* 104: 20120–20125, 2007.
- Li HC, Worrell RT, Matthews JB, Husseinzadeh H, Neumeier L, Petrovic S, Conforti L, Soleimani M. Identification of a carboxyl-terminal motif essential for the targeting of Na⁺-HCO₃⁻ cotransporter NBC1 to the basolateral membrane. *J Biol Chem* 279: 43190–43197, 2004.
- Louvard D. Apical membrane aminopeptidase appears at site of cell-cell contact in cultured kidney epithelial cells. *Proc Natl Acad Sci USA* 77: 4132–4136, 1980.
- Lytle C, Xu JC, Biemesderfer D, Forbush B, 3rd. Distribution and diversity of Na-K-Cl cotransport proteins: a study with monoclonal antibodies. *Am J Physiol Cell Physiol* 269: C1496–C1505, 1995.
- Macia E, Ehrlich M, Massol R, Boucrot E, Brunner C, Kirchhausen T. Dynasore, a cell-permeable inhibitor of dynamin. *Dev Cell* 10: 839–850, 2006.
- Marsh M. *Endocytosis*. New York: Oxford University Press, 2001, p.283.
- Mason AK, Jacobs BE, Welling PA. AP-2-dependent internalization of potassium channel Kir2.3 is driven by a novel di-hydrophobic signal. *J Biol Chem* 283: 5973–5984, 2008.
- Matlin KS, Reggio H, Helenius A, Simons K. Infectious entry pathway of influenza virus in a canine kidney cell line. *J Biol Chem* 91: 601–613, 1981.
- Matthews JB. Molecular regulation of Na⁺-K⁺-2Cl⁻ cotransporter (NKCC1) and epithelial chloride secretion. *World J Surg* 26: 826–830, 2002.

35. **Matthews JB, Awtrey CS, Hecht G, Tally KJ, Thompson RS, Madara JL.** Phorbol ester sequentially downregulates cAMP-regulated basolateral and apical Cl⁻ transport pathways in T84 cells. *Am J Physiol Cell Physiol* 265: C1109–C1117, 1993.
36. **Matthews JB, Hassan I, Meng S, Archer SY, Hrnjez BJ, Hodin RA.** Na-K-2Cl cotransporter gene expression and function during enterocyte differentiation. Modulation of Cl⁻ secretory capacity by butyrate. *J Clin Invest* 101: 2072–2079, 1998.
37. **Matthews JB, Smith JA, Nguyen H.** Modulation of intestinal chloride secretion at basolateral transport sites: opposing effects of cyclic adenosine monophosphate and phorbol ester. *Surgery* 118: 147–152, 1995.
38. **McNiven MA, Cao H, Pitts KR, Yoon Y.** The dynamin family of mechanoenzymes: pinching in new places. *Trends Biochem Sci* 25: 115–120, 2000.
39. **Miranda M, Dionne KR, Sorkina T, Sorkin A.** Three ubiquitin conjugation sites in the amino terminus of the dopamine transporter mediate protein kinase C-dependent endocytosis of the transporter. *Mol Biol Cell* 18: 313–323, 2007.
- 39a. **Moriguchi T, Urushiyama S, Hisamoto N, Iemura S, Uchida S, Natsume T, Matsumoto K, Shibuya H.** WNK1 regulates phosphorylation of cation-chloride-coupled cotransporters via the STE20-related kinases, SPAK and OSR1. *J Biol Chem* 280: 42685–42693, 2005.
40. **Mukherjee S, Ghosh RN, Maxfield FR.** Endocytosis. *Physiol Rev* 77: 759–803, 1997.
41. **Muth TR, Caplan MJ.** Transport protein trafficking in polarized cells. *Annu Rev Cell Dev Biol* 19: 333–366, 2003.
- 41a. **Payne JA, Ferrell C, Chung CY.** Endogenous and exogenous Na-K-Cl cotransporter expression in a low K-resistant mutant MDCK cell line. *Am J Physiol Cell Physiol* 280: C1607–C1615, 2001.
42. **Perry C, Quissell DO, Reyland ME, Grichtchenko II.** Electrogenic NBCe1 (SLC4A4), but not electroneutral NBCn1 (SLC4A7), cotransporter undergoes cholinergic-stimulated endocytosis in salivary ParC5 cells. *Am J Physiol Cell Physiol* 295: C1385–C1398, 2008.
43. **Reynolds A, Parris A, Evans LA, Lindqvist S, Sharp P, Lewis M, Tighe R, Williams MR.** Dynamic and differential regulation of NKCC1 by calcium and cAMP in the native human colonic epithelium. *J Physiol* 582: 507–524, 2007.
44. **Russell JM.** Sodium-potassium-chloride cotransport. *Physiol Rev* 80: 211–276, 2000.
45. **Shen L, Turner JR.** Actin depolymerization disrupts tight junctions via caveolae-mediated endocytosis. *Mol Biol Cell* 16: 3919–3936, 2005.
46. **Song JC, Hrnjez BJ, Farokhzad OC, Matthews JB.** PKC-ε regulates basolateral endocytosis in human T84 intestinal epithelia: role of F-actin and MARCKS. *Am J Physiol Cell Physiol* 277: C1239–C1249, 1999.
47. **Traub LM, Lukacs GL.** Decoding ubiquitin sorting signals for clathrin-dependent endocytosis by CLASPs. *J Cell Sci* 120: 543–553, 2007.
48. **Wang LH, Rothberg KG, Anderson RG.** Mis-assembly of clathrin lattices on endosomes reveals a regulatory switch for coated pit formation. *J Biol Chem* 268: 1107–1117, 1993.
49. **Watts C.** Rapid endocytosis of the transferrin receptor in the absence of bound transferrin. *J Biol Chem* 260: 633–637, 1985.
50. **Welker P, Böhlick A, Mutig K, Salanova M, Kahl T, Schlüter H, Blottner D, Ponce-Coria J, Gamba G, Bachmann S.** Renal Na⁺-K⁺-Cl⁻ cotransporter activity and vasopressin-induced trafficking are lipid raft-dependent. *Am J Physiol Renal Physiol* 295: F789–F802, 2008.
51. **West MA, Bretscher MS, Watts C.** Distinct endocytotic pathways in epidermal growth factor-stimulated human carcinoma A431 cells. *J Cell Biol* 109: 2731–2739, 1989.
52. **Zhang Q, Hong M, Duan P, Pan Z, Ma J, You G.** Organic anion transporter OAT1 undergoes constitutive and protein kinase C-regulated trafficking through a dynamin- and clathrin-dependent pathway. *J Biol Chem* 283: 32570–32579, 2008.

